AAPS PharmSciTech, Vol. 17, No. 3, June 2016 (© 2015)
DOI: 10.1208/s12249-015-0384-z

Research Article

Effects of Formulation Variables on the Particle Size and Drug Encapsulation of Imatinib-Loaded Solid Lipid Nanoparticles

Biki Gupta,[1] Bijay Kumar Poudel,[1] Shiva Pathak,[1] Jin Wook Tak,[1] Hee Hyun Lee,[1] Jee-Heon Jeong,[1] Han-Gon Choi,[2] Chul Soon Yong,[1,3] and Jong Oh Kim[1,3]

Received 23 June 2015; accepted 3 August 2015; published online 25 August 2015

Abstract. Imatinib (IMT), an anticancer agent, inhibits receptor tyrosine kinases and is characterized by poor aqueous solubility, extensive first-pass metabolism, and rapid clearance. The aims of the current study are to prepare imatinib-loaded solid lipid nanoparticles (IMT-SLN) and study the effects of associated formulation variables on particle size and drug encapsulation on IMT-SLN using an experimental design. IMT-SLN was optimized by use of a "combo" approach involving Plackett-Burman design (PBD) and Box-Behnken design (BBD). PBD screening resulted in the determination of organic-to-aqueous phase ratio (O/A), drug-to-lipid ratio (D/L), and amount of Tween® 20 (Tw20) as three significant variables for particle size (S_z), drug loading (DL), and encapsulation efficiency (EE) of IMT-SLN, which were used for optimization by BBD, yielding an optimized criteria of O/A=0.04, D/L=0.03, and Tw20=2.50%*w*/*v*. The optimized IMT-SLN exhibited monodispersed particles with a size range of 69.0±0.9 nm, ζ-potential of −24.2±1.2 mV, and DL and EE of 2.9±0.1 and 97.6±0.1%*w*/*w*, respectively. Results of *in vitro* release study showed a sustained release pattern, presumably by diffusion and erosion, with a higher release rate at pH 5.0, compared to pH 7.4. In conclusion, use of the combo experimental design approach enabled clear understanding of the effects of various formulation variables on IMT-SLN and aided in the preparation of a system which exhibited desirable physicochemical and release characteristics.

KEY WORDS: Box-Behnken design; imatinib; Plackett-Burman design; response surface methodology; solid lipid nanoparticle.

INTRODUCTION

Imatinib (IMT) is an inhibitor of receptor tyrosine kinases with highly potent and specific inhibitory activity against BCR-ABL fusion gene, platelet-derived growth factor receptor (PDGFR), and c-KIT receptor (1). The highly specific anti-proliferative activity of IMT provides strong foundations for its applications to targeted cancer chemotherapy. However, the free base of IMT is practically insoluble in water (0.001 g/100 ml), undergoes extensive first-pass metabolism by cytochrome P450 enzymes, and shows rapid clearance with an elimination half-life of ~18 h (2), which lead to poor bioavailability, ultimately limiting its applicability to clinical settings (3). The mesylate salt of IMT, which is marketed by Novartis as Gleevec®, has been approved by FDA for the treatment of Philadelphia chromosome-positive chronic myeloid leukemia (Ph^+ CML), myelodysplastic/ myeloproliferative diseases associated with PDGFR gene rearrangements, aggressive systemic mastocytosis, hypereosinophilic syndrome, chronic eosinophilic leukemia, dermatofibrosarcoma protuberans, and malignant gastrointestinal stromal tumors (4).

Solid lipid nanoparticles (SLNs), which are lipid-based nanocarriers composed of a solid lipid core, have been studied extensively in recent years for use in the administration of a large variety of drugs and genetic materials, as monotherapy and in combination, by various routes of administration (5–14). Such extensive investigations of SLN have been encouraged by the fact that SLN combines the characteristics of different carrier systems, without the various drawbacks often associated with conventional carrier systems. Accordingly, tremendous potential of SLNs to overcome bioavailability issues of drugs exhibiting poor aqueous solubility, extensive first-pass metabolism, and/or rapid renal clearance has been demonstrated. Consequently, SLNs are considered to have great potential for delivery of such medications *via* oral, parenteral, and other routes of administration (3,6).

Design of experiments (DoE) approach has been an extremely useful tool for defining design spaces around individual or multiple unit operations, which is an important component of control strategy for quality by design (QbD) (15). DoE can be used in construction of a predictive model of the critical response variables, thereby facilitating identification of all potential independent variables and their

[1] College of Pharmacy, Yeungnam University, 214-1, Dae-Dong, Gyeongsan, 712-749, South Korea.
[2] College of Pharmacy, Institute of Pharmaceutical Science and Technology, Hanyang University, 55, Hanyangdaehak-ro, Sangnok-gu, Ansan, 426-791, South Korea.
[3] To whom correspondence should be addressed. (e-mail: csyong@yu.ac.kr; jongohkim@yu.ac.kr)

simultaneous systematic and rapid evaluation (16). Optimization strategy for a multivariate process, particularly where the number of variables is extremely large, requires an experimental design consisting of an initial screening (usually by fractional factorial design and Plackett-Burman design), followed by optimization using a response surface design, such as Box-Behnken design and central composite design (17,18).

The current study used a "combo" experimental design approach utilizing Plackett-Burman design and Box-Behnken design for the optimization and preparation of SLN loaded with IMT as an anticancer agent having poor aqueous solubility for characterization of the optimized IMT-SLN and study of its *in vitro* release characteristics.

MATERIALS AND METHODS

Materials

IMT was obtained from LC Laboratories (Woburn, MA, USA). Precirol® ATO 5 (PcA, glyceryl distearate) was obtained from Gattefosse (St. Priest, France), while Tween® 20 (TwN, polysorbate 20) and lecithin (LcN) were purchased from Samchun Chemicals (Seoul, Korea) and Junsei (Tokyo, Japan), respectively. Deionized water was freshly prepared as per requirement using a Milli-Q water purification system (Millipore, MA, USA). Other chemicals were reagent grade and were used without further purification.

Methods

HPLC Analysis for Imatinib

Method for quantification of IMT was developed by modification of a previously reported HPLC method (19). The HPLC system (Hitachi, Tokyo, Japan) consisted of an L-2130 pump, an L-2200 autosampler, an L-2420 UV–vis detector, and an L-2350 column oven devised using EZChrom elite software (version 318a). An Inertsil C_8 column (250×4.6 mm, 5 μm particle size; GL Sciences Inc., Tokyo, Japan) was employed under isocratic elution using 0.02 M monobasic potassium phosphate/acetonitrile (6:4, *v/v*) as the mobile phase at a flow rate of 1.0 ml/min and column temperature of 25.0±1.0°C. For each analysis, a 20-ml aliquot of the sample was injected and the UV absorbance was measured at a wavelength of 265 nm. The calibration plots exhibited exceptional linearity (R^2=0.999) over a concentration range of 0.1–100 μg/ml and the relative standard deviation (RSD) of the plot over different periods of time was below 3%.

Preparation of IMT-SLN

IMT-SLN was prepared by *hot homogenization method* consisting of homogenization and sonication. The method was developed by modification of previously reported methods for preparation of SLN (5–7,20–23). Briefly, the solid lipid (PcA) was dissolved at 70°C and mixed with LcN to constitute the organic phase, to which IMT was added and dissolved by stirring at 50 rpm for 10 min. For the aqueous phase, TwN was dissolved in purified water and heated to 70°C. The aqueous phase was added to the organic phase using a 10-ml disposable syringe and homogenized using high-performance homogenizer (ULTRA-TURRAX® T25, IKA). The resulting primary emulsion was sonicated using a probe sonicator (Vibra-Cell™, SONICS) and cooled in an ice bath for 3 h to obtain IMT-SLN. Blank SLN was prepared using the same procedure, omitting the addition of IMT.

Plackett-Burman Design

An 11-factor Plackett-Burman design (PBD) at two levels was utilized for initial screening of the main effects of seven variables (Table I) on particle size (S_z; y_1), drug loading (DL; y_2), and encapsulation efficiency (EE; y_3) of IMT-SLN. The lower and upper levels of the seven variables were selected on the basis of prior preliminary experiments. Using Design-Expert® 8.0.7.1 software (Stat-Ease Inc., Minneapolis, MN, USA), 12 experimental runs were generated and were conducted randomly. Variables that exhibited significant main effects by PBD on the specified responses were selected for further optimization of main effects, interaction effects, and quadratic effects by Box-Behnken design.

Box-Behnken Design

A three-factor Box-Behnken design (BBD) was employed to optimize the main effects, interaction effects, and quadratic effects of the formulation variables on S_z (Y_1), DL (Y_2), and EE (Y_3) of IMT-SLN. The upper and lower levels, along with the central point, of the three variables are shown in Table I. Using Design-Expert® software, 17 experimental runs were generated, which included five center point replicates. The purpose of inclusion of the recommended center point replicates is to ensure that the design gives a good estimate of experimental error and to provide an accurate test for lack of fit. The results for each of the response factors were fitted to a quadratic polynomial model described by the following non-linear equation.

$$Y = \beta_0 + \beta_1 X_1 + \beta_2 X_2 + \beta_3 X_3 + \beta_4 X_1 X_2 + \beta_5 X_1 X_3 + \beta_6 X_2 X_3 + \beta_7 X_1^2 + \beta_8 X_2^2 + \beta_9 X_3^2$$

Table I. Variables for Plackett-Burman Design and Box-Behnken Design

Plackett-Burman design			
Variables		Lower level	Upper level
x_1: organic-to-aqueous phase ratio, O/A		0.04	0.06
x_2: drug-to-lipid ratio, D/L		0.01	0.03
x_3: amount of lecithin, Lec[a]		2.5%*w/w*	7.5%*w/w*
x_4: amount of Tween 20, Tw20[b]		1.5%*w/v*	2.5%*w/v*
x_5: homogenization time, HT		5 min	15 min
x_6: sonication time, ST		8 min	12 min
x_7: sonication amplitude, SA		60%	80%
Box-Behnken design			
Variables	Central point	Lower level	Upper level
X_1: O/A	0.05	0.04	0.06
X_2: D/L	0.02	0.01	0.03
X_3: Tw20[b]	2.0%*w/v*	1.5%*w/v*	2.5%*w/v*

[a] Relative to lipid amount
[b] Relative to aqueous phase

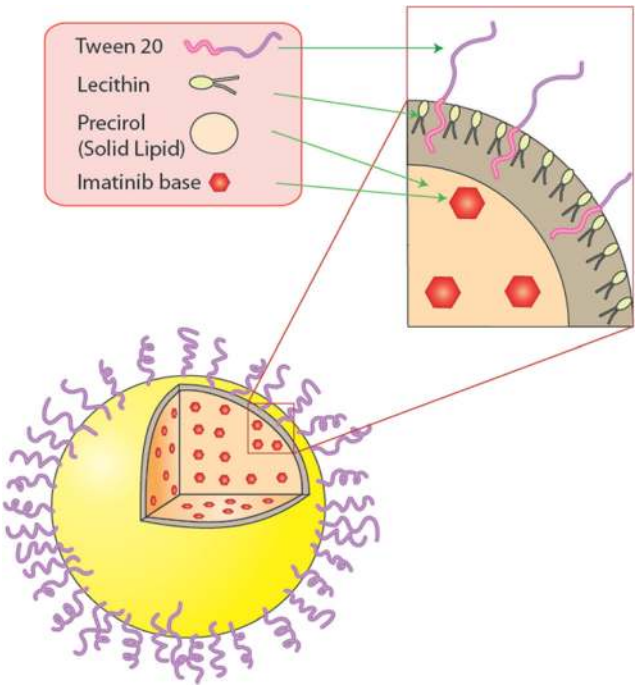

Fig. 1. The scheme of imatinib-loaded solid lipid nanoparticles (IMT-SLN)

where Y is the individual response factor or dependent variable; β_0–β_9 are regression coefficients; and X_1, X_2, and X_3 are the independent variables.

Optimization Using Desirability Functions

Following establishment of relationships between dependent and independent variable *via* model polynomials, all three responses were optimized by use of the desirability functions approach (24) using Design-Expert® software. Using the desirability functions approach, each response i is associated with its own partial desirability function (d_i), which varies from 0 to 1 depending on the closeness of the response to its target value, *i.e.*, desirability equal to 0 corresponds to the point farthest from the target value while that equal to 1 corresponds to the point closest to the target value.

For maximization of response, the desirability function can be defined as

$$d_i = \{(Y_i - Y_{\min})/(Y_{\max} - Y_{\min})\}^s$$

For minimization of response, the desirability function can be defined as

$$d_i = \{(Y_{\max} - Y_i)/(Y_{\max} - Y_{\min})\}^t$$

Here, d_i represents individual desirability of the response, Y_i represents the experimental value of the response, and $Y_{\min}$ and $Y_{\max}$ represent the minimum and maximum acceptable values of the response, respectively. The values of s and t (varying from 0.1 to 10) are specified depending on how close the solution is desired from the stated target, *i.e.*, a value of 10 will cause the optimization to seek a solution close to or beyond the stated target. For the purpose of optimization of the IMT-SLN formulation, a value of 1 was specified to both s and t.

Particle Size, Polydispersity Index, and ζ-Potential

The hydrodynamic size, polydispersity index (PDI), and ζ-potential of the IMT-SLN system was determined by dynamic light scattering (DLS) technique using a Nano-S90 ZetaSizer (Malvern Instruments, Worcestershire, UK). The measurements were performed at a fixed scattering angle of 90° and at an equilibrated temperature of 25°C. Each sample was adequately diluted with distilled water prior to measurement, and three measurements were performed for each sample.

Drug Loading and Encapsulation Efficiency

DL and EE were determined by ultracentrifugation. A 2-ml aliquot of IMT-SLN was placed in an Amicon® Ultra-4 10K centrifugal filter device (molecular weight cutoff 10 kDa;

Table II. Plackett-Burman Design Matrix and Observed Response Values

Run	x_1	x_2	x_3 (%*w*/*w*)	x_4 (%*w*/*v*)	x_5 (min)	x_6 (min)	x_7 (%)	x_8	x_9	x_{10}	x_{11}	y_1 (nm)	PDI	y_2 (%*w*/*w*)	y_3 (%*w*/*w*)
1	0.04	0.03	2.5	2.5	15	8	80	1	1	−1	−1	65.13	0.217	2.94	97.89
2	0.06	0.03	2.5	2.5	15	12	60	−1	−1	1	−1	109.17	0.248	2.96	98.54
3	0.06	0.03	7.5	1.5	5	8	80	−1	1	1	−1	160.33	0.236	2.95	98.35
4	0.04	0.03	7.5	1.5	15	12	80	−1	−1	−1	1	108.33	0.242	2.93	97.55
5	0.06	0.01	2.5	1.5	15	8	80	1	−1	1	1	169.67	0.227	0.95	95.28
6	0.06	0.01	7.5	2.5	15	8	60	−1	1	−1	1	119.57	0.239	0.98	97.74
7	0.04	0.01	2.5	1.5	5	8	60	−1	−1	−1	−1	126.70	0.232	0.96	95.93
8	0.04	0.03	7.5	2.5	5	8	60	1	−1	1	1	83.33	0.260	2.94	98.14
9	0.06	0.01	7.5	2.5	5	12	80	1	−1	−1	−1	102.80	0.222	0.96	95.50
10	0.04	0.01	2.5	2.5	5	12	80	−1	1	1	1	61.19	0.206	0.97	96.59
11	0.06	0.03	2.5	1.5	5	12	60	1	1	−1	1	167.83	0.232	2.94	98.07
12	0.04	0.01	7.5	1.5	15	12	60	1	1	1	−1	114.93	0.220	0.96	96.03

x_1 organic-to-aqueous phase ratio (O/A); x_2 drug-to-lipid ratio (D/L); x_3 amount of lecithin (Lec); x_4 amount of Tween® 20 (Tw20); x_5 homogenization time (HT); x_6 sonication time (ST); x_7 sonication amplitude (SA); x_8, x_9, x_{10}, and x_{11} dummy variables; y_1 particle size (S_z); y_2 drug loading (DL); y_3 encapsulation efficiency (EE)

Merck Millipore Ltd., Ireland), centrifuged at 2000*g* for 10 min, and the filtrate was analyzed for free drug by HPLC quantification as described in the previous section. DL and EE were calculated using the following formulae:

$$DL(\%) = \{(W_T - W_U)/(W_L + W_T - W_U)\}*100$$
$$EE(\%) = \{(W_T - W_U)/W_T\}*100$$

Here, W_T, W_U, and W_L denote weight of initially added total drug, weight of unbound drug, and weight of total lipid, respectively.

Transmission Electron Microscopy

Transmission electron microscopy (TEM) was employed to examine the size and morphology of the IMT-SLN. A drop of the formulation was deposited onto a copper grid coated with a carbon film, and the particles were subjected to negative staining by 2%*w/v* phosphotungstic acid. The sample was then appropriately dried under mild to moderate infrared radiation and observed under an H7600 transmission electron microscope (Hitachi, Tokyo, Japan).

Freeze-Drying

IMT-SLN, along with blank SLN, was pre-frozen at −70°C for 6 h and subsequently lyophilized (freeze-dried) at −40°C for 24 h using an EYELA® Freeze Dryer (Tokyo Rikakikai Co. Ltd., Tokyo, Japan). Upon completion of freeze-drying, the samples were allowed to dry for an additional 12 h at 20°C.

Differential Scanning Calorimetry

Freeze-dried IMT-SLN and blank SLN were used for solid-state characterization by differential scanning calorimetry (DSC). A DSC-Q200 differential scanning calorimeter (TA Instruments, New Castle, DE, USA) was used for observation of thermal characteristics of IMT-SLN, blank SLN, and IMT. DSC scans were performed by heating all samples from 20 to 250°C, at a heating rate of 20°C/min in a dynamic nitrogen atmosphere.

X-Ray Diffraction

A vertical goniometer and X-ray diffractometer (X'pert PRO MPD diffractometer, Almelo, The Netherlands) was used to observe the X-ray diffraction (XRD) patterns of freeze-dried IMT-SLN, blank SLN, and IMT. The diffractometer measured Ni-filtered CuKα-radiation (voltage 40 kV; current 30 mA) scattered in the crystalline regions of the sample. XRD scans were performed over a diffraction angle (2θ) range of 10–60° and a scanning rate of 5°/min.

Physical Stability Study

Physical stability of the IMT-SLN system was assessed by recording changes in S_z, PDI, and EE over a period of 60 days upon storage at two different temperatures, 4 and 22°C. An aliquot of the sample was taken after 0, 1, 2, 4, 7, 15, 30, and 60 days of storage and S_z/PDI and EE were determined by DLS characterization and centrifugation method, respectively.

In Vitro Release Study

In vitro release study was performed by dialysis method at pH 7.4 and pH 5.0, using phosphate-buffered saline (PBS) and acetate buffer solution (ABS) as respective release media. Briefly, 2 ml aliquots of IMT-SLN (equivalent to 2.5 mg of IMT) were placed in dialysis bags (molecular weight cutoff

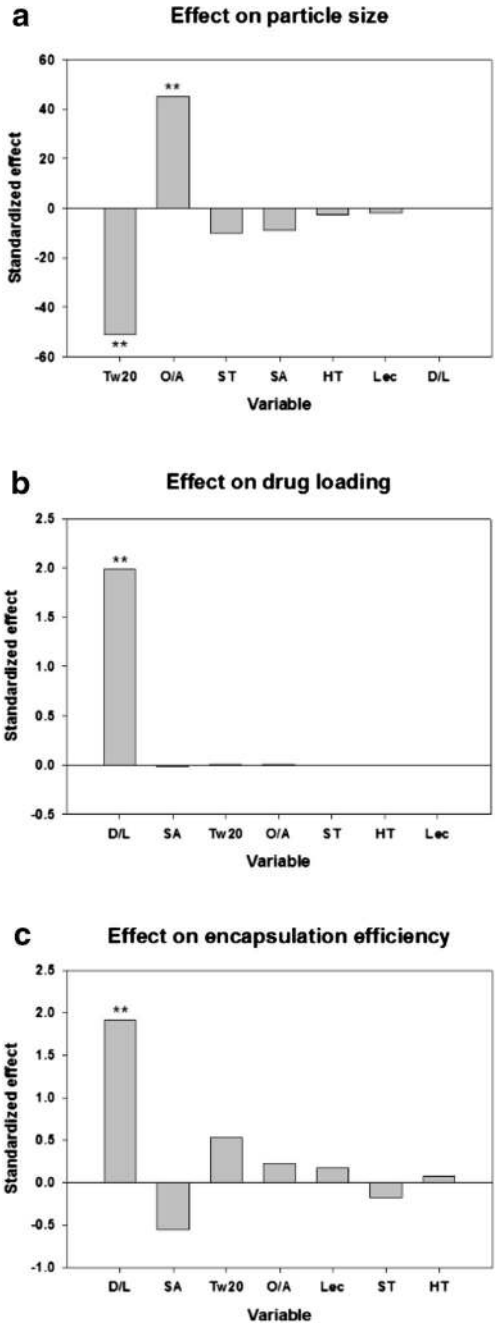

Fig. 2. Plackett-Burman Design: effects of different variables on particle size (**a**), drug loading (**b**), and encapsulation efficiency (**c**). **Significant at $p<0.001$. *O/A* organic-to-aqueous phase ratio, *D/L* drug-to-lipid ratio, *Tw20* amount of Tween® 20, *Lec* amount of lecithin, *HT* homogenization time, *ST* sonication time, *SA* sonication amplitude

Table III. Box-Behnken Design Matrix and Observed Response Values

Run	X_1	X_2	X_3 (%*w*/*v*)	Y_1 (nm)	PDI	Y_2 (%*w*/*w*)	Y_3 (%*w*/*w*)
1	0.05	0.02	2.0	108.00	0.221	1.95	97.38
2	0.04	0.02	1.5	112.60	0.220	1.92	96.24
3	0.05	0.03	1.5	138.23	0.218	2.92	97.47
4	0.06	0.01	2.0	126.27	0.207	0.96	95.52
5	0.05	0.02	2.0	102.33	0.220	1.94	97.18
6	0.06	0.02	2.5	104.60	0.211	1.94	96.99
7	0.04	0.02	2.5	70.80	0.208	1.95	97.70
8	0.04	0.03	2.0	89.08	0.225	2.94	97.91
9	0.04	0.01	2.0	89.72	0.205	0.98	97.60
10	0.05	0.03	2.5	88.55	0.223	2.95	98.28
11	0.05	0.02	2.0	106.67	0.220	1.95	97.61
12	0.06	0.02	1.5	156.37	0.210	1.95	97.55
13	0.05	0.01	1.5	139.87	0.237	0.96	95.59
14	0.06	0.03	2.0	134.07	0.256	2.96	98.58
15	0.05	0.02	2.0	110.13	0.231	1.96	98.01
16	0.05	0.02	2.0	109.70	0.238	1.95	97.62
17	0.05	0.01	2.5	91.10	0.213	0.96	96.24

X_1 organic-to-aqueous phase ratio (O/A), X_2 drug-to-lipid ratio (D/L), X_3 amount of Tween® 20 (Tw20); Y_1 particle size (S_z), Y_2 drug loading (DL), Y_3 encapsulation efficiency (EE)

Table IV. ANOVA for the Response Surface Reduced Quadratic Models

Response	Source	Sum of squares	Mean square	*F* value	*p* value
Y_1: particle size	Model	7887.80	1577.56	166.70	<0.0001
	X_1: O/A	3164.37	3164.37	334.37	<0.0001
	X_2: D/L	1.11	1.11	0.12	0.7390
	X_3: Tw20	4608.64	4608.64	486.99	<0.0001
	X_2^2	34.48	34.48	3.64	0.0827
	X_3^2	73.27	73.27	7.74	0.0178
	Residual	104.10	9.46		
	Lack of fit	64.77	9.25	0.94	0.5587*
	Pure error	39.32	9.83		
	Cor total	7991.90			
Y_2: drug loading	Model	7.84	1.12	35,093.73	<0.0001
	X_1: O/A	1.52×10^{-5}	1.52×10^{-5}	0.48	0.5075
	X_2: D/L	7.84	7.84	2.456×10^{5}	<0.0001
	X_3: Tw20	2.975×10^{-4}	2.975×10^{-4}	9.32	0.0137
	X_1X_2	4.145×10^{-4}	4.145×10^{-4}	12.99	0.0057
	X_1X_3	4.058–10^{-4}	4.058×10^{-4}	12.72	0.0061
	X_2^2	1.176×10^{-4}	1.176×10^{-4}	3.69	0.0871
	X_3^2	3.267×10^{-4}	3.267×10^{-4}	10.24	0.0108
	Residual	2.871×10^{-4}	3.19×10^{-5}		
	Lack of fit	1.341×10^{-4}	2.683×10^{-5}	0.70	0.6522*
	Pure error	1.53×10^{-4}	3.825×10^{-5}		
	Cor total	7.84			
Y_3: encapsulation efficiency	Model	11.31	1.88	16.557	0.0001
	X_1: O/A	0.084	0.084	0.74	0.4093
	X_2: D/L	6.64	6.64	58.39	<0.0001
	X_3: Tw20	0.69	0.69	6.10	0.0331
	X_1X_2	1.88	1.88	16.57	0.0022
	X_1X_3	1.01	1.01	8.92	0.0136
	X_3^2	0.99	0.99	8.72	0.0145
	Residual	1.14	0.11		
	Lack of fit	0.75	0.13	1.31	0.4129*
	Pure error	0.38	0.096		
	Cor total	12.44			

Insignificant factors were excluded from the model to obtain a better fit
*Not significant at $p<0.1$

Table V. Correlation Coefficients for the Response Surface Reduced Quadratic Models

Response	R^2	Adjusted R^2	Predicted R^2	Adeq precision
Y_1	0.9870	0.9811	0.9678	48.030
Y_2	1.0000	0.9999	0.9999	517.667
Y_3	0.9086	0.8538	0.5898	14.764

3.5 kD), previously hydrated overnight in respective release media. The dialysis bags were clipped at both ends and then kept in a USP Type II dissolution apparatus containing 400 ml of respective release media (with 1%*w*/*v* TwN), maintained at a temperature of 37±0.5°C. The paddles were operated at 50 rpm, and 2 ml of the medium was withdrawn at defined time intervals and replaced with the same amount of fresh release medium each time. HPLC was performed to determine the content of IMT in each sample.

Statistical Analysis

All data were expressed as mean±SD (n=3). Data obtained from the experiments designed using Box-Behnken design were analyzed by ANOVA, lack-of-fit tests, and multiple correlation coefficients. Student's t test was used to test the statistical significance wherever applicable.

RESULTS AND DISCUSSION

Preparation of IMT-SLN

Hot homogenization technique was employed for preparation of IMT-SLN, which involved homogenization and subsequent probe sonication. While the solid lipid core was composed of glyceryl distearate (PcA), LcN was used as a hydrophobic emulsifier. In addition, TwN (polysorbate 20), a polyoxyethylene derivative, was used as a hydrophilic surfactant. The hydrophilic polyoxyethylene polymer, along with the hydrophobic LcN, confers a highly protective amphiphilic stealth outer cover to the SLN, which provides long-circulating properties to the carrier system by evading clearance by the reticuloendothelial system (25,26). The long-circulating carriers act as circulating drug reservoirs in blood and aid passive targeting. These characteristics are highly beneficial for cancer chemotherapy (27). The scheme of the IMT-SLN system is shown in Fig. 1.

Plackett-Burman Design

PBD was used for screening variables among the lot which showed no significant influence on SLN characteristics. PBD is a two-level screening design, which enables the examination of a relatively large number of variables in a relatively small number of experiments (17). It is recommended for study of the main effects, assuming absence of interaction effects. It is also useful for ruggedness testing, where the aim is to determine whether the given factors have little or no impact on a given response. An 11-factor PBD was employed to study the main effects of the seven independent variables, employing four dummy variables to make up the 11 factors. The PBD matrix generated using Design-Expert® software, along with the observed response values, has been shown in Table II. The respective PDI for each of the 12 runs, which were highly acceptable (<0.300) in all cases, are also included in the table. The effects of the seven independent variables on S_z, DL, and EE are illustrated in Fig. 2. As evident from the illustration, amount of Tween® 20 (Tw20) and organic-to-aqueous phase ratio (O/A) showed significant main effects on S_z, while drug-to-lipid ratio (D/L) showed significant main effects on DL and EE. Based on this observation, O/A, D/L, and Tw20 were selected as three variables for further optimization by employing Box-Behnken design.

Box-Behnken Design

The most significant factors, usually after determination from a screening experiment or from experience, are subjected to detailed examination using a suitable response surface design approach to obtain optimal conditions for each factor (17). Therefore, BBD was used to optimize the main effects, interaction effects, and quadratic effects of three independent variables, *viz*. O/A (X_1), D/L (X_2), and Tw20 (X_3) on three response variables, S_z (Y_1), DL (Y_2), and EE (Y_3). The 17 experimental runs, generated using Design-Expert® software, were as represented by the BBD matrix in Table III. The runs, as entailed by the BBD matrix, were conducted simultaneously. The corresponding values of the response variables observed were as summarized alongside each run in the BBD matrix shown in Table III, which also includes the corresponding PDI values. Each response was individually fitted to a second-order quadratic model. Various statistical parameters

Table VI. Factor Coefficient Estimates and Corresponding Standard Error Values

Factor	Y_1		Y_2		Y_3	
	Coeff. estimate	Std. error	Coeff. estimate	Std. error	Coeff. estimate	Std. error
Intercept	107.17	1.22	1.95	2.24×10^{-3}	97.49	0.11
X_1	19.89	1.09	1.38×10^{-3}	2.00×10^{-3}	−0.01	0.12
X_2	0.37	1.09	0.99	2.00×10^{-3}	0.91	0.12
X_3	−24.00	1.09	6.10×10^{-3}	2.00×10^{-3}	0.29	0.12
X_1X_2	–	–	0.010	2.82×10^{-3}	0.69	0.17
X_1X_3	–	–	−0.010	2.82×10^{-3}	−0.50	0.17
X_2^2	2.86	1.50	5.28×10^{-3}	2.75×10^{-3}	–	–
X_3^2	4.17	1.50	-8.80×10^{-3}	2.75×10^{-3}	−0.48	0.16

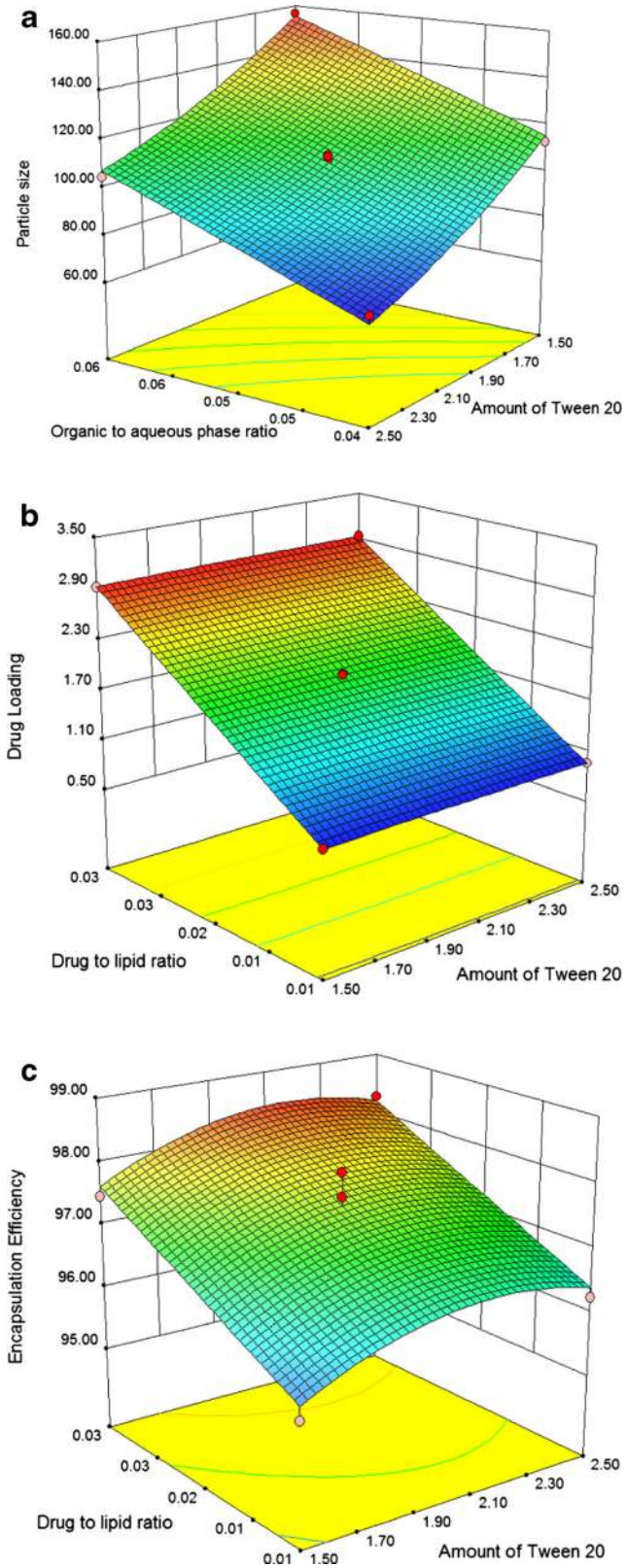

Fig. 3. Box-Behnken Design: 3-D response surface plots showing **a** effects of organic-to-aqueous phase ratio and amount of Tween® 20 on particle size, **b** effects of drug-to-lipid ratio and amount of Tween® 20 on drug loading, and **c** effects of drug-to-lipid ratio and amount of Tween® 20 on encapsulation efficiency

provided by software, comprising ANOVA, lack-of-fit tests, and multiple correlation coefficients (R^2) tests, were used to determine the model significance. Results of such statistical evaluations are shown in Tables IV and V.

At a significance level of 5%, models corresponding to all three responses, Y_1, Y_2, and Y_3, showed a good fit to the quadratic model, as can be confirmed by their respective model p values shown in Table IV. In addition, the lack of fit for each model was insignificant (p value >0.1). Insignificant lack of fit is desirable to reaffirm that a model exhibits good fitting to the corresponding response. The correlation coefficient (R^2) value and the adequate precision value, a measure of signal to noise ratio, were also adequately large for each of the three responses (Table V). The significant individual model terms are also included in Table IV. The factor terms X_2^2 and X_3^2 indicate quadratic effects while X_1X_2 and X_1X_3 indicate interaction effects. To ensure a better fit, factor terms representative of interaction and quadratic effects insignificant at $p<0.1$ have been excluded from the model. From Table IV, we can observe that O/A (X_1) and Tw20 (X_3) exhibit significant main effects on S_z (Y_1) at $p<0.05$, with Tw20 having a slightly more prominent main effect on S_z than O/A as indicated by its relatively larger F value. Tw20 also exhibits significant quadratic effects (X_3^2) on S_z at $p<0.05$. Similarly, D/L (X_2) and Tw20 (X_3) exhibited significant main effects on DL (Y_2) as well as EE (Y_3) at $p<0.05$. O/A-D/L (X_1X_2) and O/A-Tw20 (X_1X_3) exhibited significant interaction effects, while Tw20 (X_3^2) exhibited significant quadratic effects on both DL and EE at $p<0.05$.

Factor coefficients representing quantitative effects of the independent variables X_1, X_2, and X_3 on the responses Y_1, Y_2, and Y_3 are shown in Table VI, which, upon consideration along with the findings of the prior statistical evaluations, prompt the conclusion that X_1 had a significant positive main effect and X_3 had a significant negative main effect on Y_1, while X_2 and X_3 had significant positive main effects on both Y_2 and Y_3. X_1–X_2 had significant positive interaction effects on both Y_2 and Y_3, while X_1–X_3 had significant negative interaction effects on both Y_2 and Y_3. X_3 had a significant positive quadratic effect on Y_1, while it had a significant negative quadratic effect on Y_2 and Y_3. All observations were in good agreement with those of previously reported studies (28–30).

Response Surface Analysis

Response surface analysis, aided by three-dimensional response surface plots (Fig. 3), was employed to further elucidate the relationships between the dependent and

Table VII. Predicted and Observed Response Values for Optimized Formulation

Response	Prediction	Standard error of prediction	Observation[a]
Y_1: particle size (nm)	70.80	*3.83*	69.04±0.94[b]
Y_2: drug loading (%*w*/*w*)	2.94	*0.01*	2.93±0.002[b]
Y_3: encapsulation efficiency (%*w*/*w*)	98.13	*0.58*	97.60±0.05[b]

[a] Values are expressed as mean±SD (n=3)
[b] No significant difference from the predicted response values at $p<0.05$

independent variables deemed statistically significant. A 3-D response surface plot is a graphical representation of a regression equation exhibiting changes in response variable against two independent variables at a time, keeping the other variables fixed at their middle levels. Figure 3a depicts the effects of O/A and Tw20 on S_z, where S_z increases with an increase in O/A while it decreases with an increase in Tw20. This was in good agreement with previous reports (28,30,31). The reason for increase in S_z with increase in O/A could be that viscosity of the dispersion increases with increase in lipid fraction, leading to higher surface tension and ultimately larger particle size. The reason for decrease in S_z as a result of increased Tw20 could be that higher content of surfactant reduces the interfacial tension more effectively, thereby resulting in smaller particle sizes (28). Figure 3b depicts the effects of D/L and Tw20 on DL, where DL increases with an increase in D/L, in line with previous study reports (28,29,31). Figure 3c depicts the effects of D/L and Tw20 on EE, where with an increase in D/L, EE also increases; with an increase in Tw20, EE initially increases and then decreases. The results of EE were also in good agreement with those of previously reported studies (28).

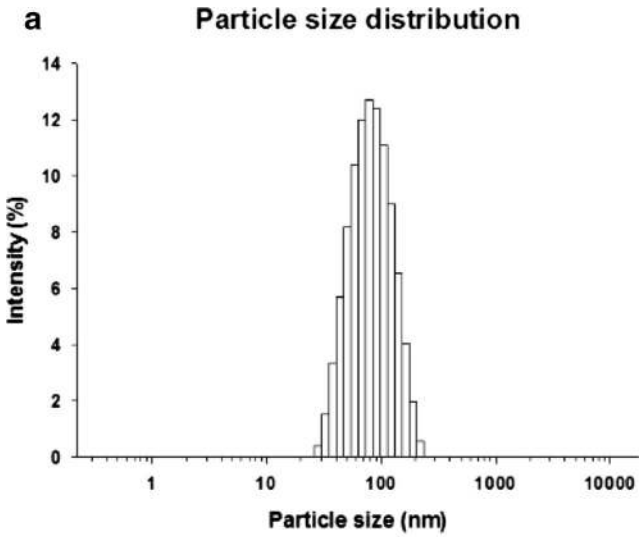

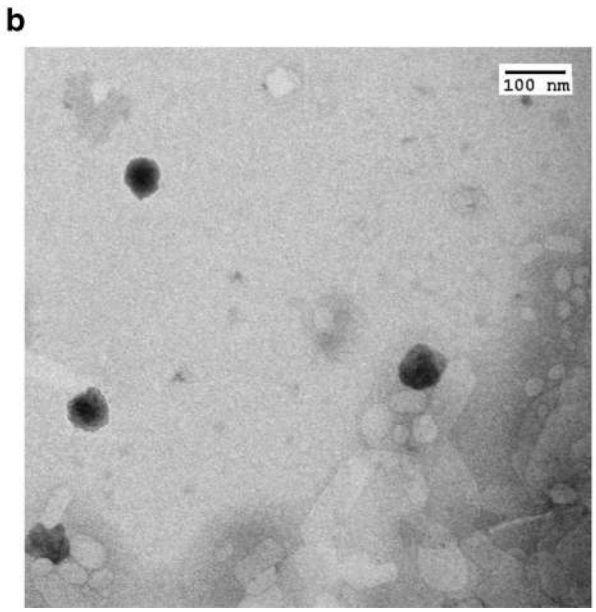

Fig. 4. Characterization of the IMT-SLN system: **a** particle size distribution and **b** transmission electron microscopy (TEM) imaging

Optimization Using Desirability Function

Generation of model polynomials to establish the relationship between dependent and independent variables was followed by subsequent optimization of the three responses using a desirability function approach for optimization of multiple responses introduced by Derringer and Suich. The three responses Y_1, Y_2, and Y_3 were transformed into individual desirability d_1, d_2, and d_3, respectively. All three variables, X_1, X_2, and X_3, were set in range and goals were defined for each response. The goal defined for Y_1 was minimization, while the goal for Y_2 and Y_3 was maximization. Equal weights and importance were assigned to each of the three responses. Consequently, a number of solutions, ordered by their desirability value, were generated. The solution showing the

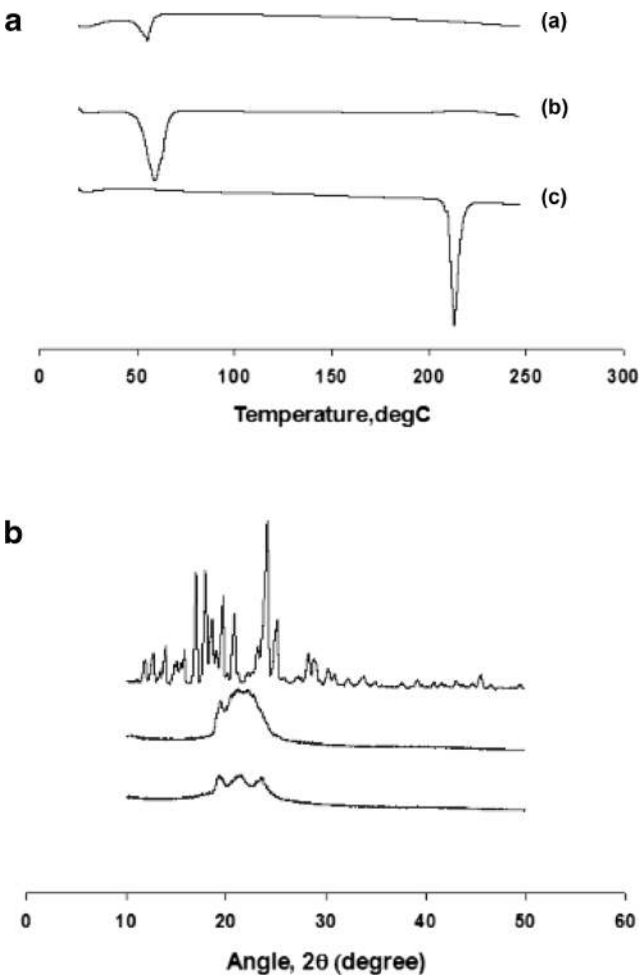

Fig. 5. Characterization of the IMT-SLN system: **a** differential scanning calorimetry (DSC) thermograms and **b** X-ray diffraction (XRD) patterns. *a* IMT-SLN, *b* Precirol ATO5, and *c* free IMT

Table VIII. Physical Stability of IMT-Loaded SLN System After Storage

Day	Upon storage at 4°C			Upon storage at 22°C		
	Particle size, nm	PDI	EE, %*w*/*v*	Particle size, nm	PDI	EE, %*w*/*v*
0	69.04±0.94	0.219±0.015	97.60±0.05	69.04±0.94	0.219±0.015	97.60±0.05
1	69.42±0.74	0.211±0.014	97.60±0.06	70.18±0.44	0.223±0.014	97.49±0.05
2	69.82±0.44	0.220±0.015	97.58±0.06	70.67±0.57	0.224±0.023	96.47±0.01
4	70.49±0.45	0.225±0.024	97.57±0.03	72.01±0.80	0.246±0.024	95.30±0.08
7	70.73±0.41	0.235±0.010	97.51±0.02	75.68±0.39	0.283±0.040	95.08±0.08
15	70.96±0.93	0.237±0.006	97.44±0.07	86.28±0.28	0.304±0.057	93.83±0.15
30	71.55±1.01	0.233±0.005	97.36±0.05	94.80±0.19	0.297±0.029	92.33±0.09
60	72.43±0.78	0.234±0.008	97.15±0.09	109.76±0.78	0.319±0.042	91.17±0.32

All observed values are expressed as mean±SD
PDI polydispersity index, *EE* encapsulation efficiency

maximum desirability value (D=0.947) was selected as the most optimum, where O/A, D/L, and Tw20 were 0.04, 0.03, and 2.50%*w*/*v*, respectively. To validate the prediction capability of the model, three optimized formulations with the above "most optimum" factor combination were prepared, and S_z, DL, and EE for each formulation were evaluated. Tabulation of the observed responses along with the predicted response values is shown in Table VII. As shown in Table VII, all of the observed response values were in good agreement with the predicted values, with reference to the standard error of prediction. This indicates that the experimental design approach closely predicted the relationships between the dependent and independent variables and was helpful in establishing a model for successful optimization of the IMT-SLN system.

Characterization of IMT-SLN

The particle size distribution of the optimized IMT-SLN system is shown in Fig. 4a. The particles showed an excellent size of 69.0±0.9 nm, with PDI within an acceptable range of 0.219±0.015. The ζ-potential of the optimized system, which is indicative of surface charge of the particles, was −24.2±1.2, and DL and EE were 2.9±0.1 and 97.6±0.1, respectively. TEM images of the IMT-SLN system are shown in Fig. 4b, which clearly illustrate that the particles were distinct and spherical and had an average size of approximately 70 nm, consistent with the data obtained by DLS characterization. The spectacularly small particle size of IMT-SLN was potentially advantageous for passive tumor targeting of the drug specifically to the tumor tissues by enhanced permeability and retention (EPR) effect. Nanocarriers with particle sizes below 200 nm are reported to be ideally suitable for exploitation of the EPR effect (32,33).

DSC and XRD constituted the solid-state characterization of IMT-SLN. As illustrated in Fig. 5a, a sharp endothermic peak was observed in the region of 211–216°C for free IMT, which represents the temperature range corresponding to the melting point of the drug. No such peak was observed in the case of IMT-SLN, rather a small endothermic peak was observed close to 55–60°C, which could be associated with that of the solid lipid. The disappearance of the endothermic peak associated with free drug in the case of IMT-SLN supported the assumption that the drug was well encapsulated within the carrier system either in molecularly dispersed state or in amorphous state (13,33). XRD pattern of IMT-SLN, along with XRD patterns of free IMT and PcA, is shown in Fig. 5b. As can be clearly observed in Fig. 5b, characteristic peaks associated with IMT appeared at 17.2, 18.1, 19.7, 21.1, 24.2, and 25.3, which were in agreement with data from a previous report (2). These characteristic peaks did not appear in the case of IMT-SLN, which provided additional support to the assumption that the drug was well encapsulated within the carrier system either in molecularly dispersed state or in amorphous state (33).

Physical Stability Study

To observe the physical stability profile of the system, physical stability study on the IMT-SLN system was conducted over a period of 60 days upon storage at temperatures of 4 and 22°C.

Tabulation of the variations in S_z, PDI, and EE over the period of storage is shown in Table VIII. As shown in the table, while the system showed minimal changes in terms of S_z, PDI, or EE, and thereby, exceptional stability upon storage at 4°C, it showed marginal changes in S_z, PDI, and EE upon storage at 22°C. This behavior of the system was expected, as upon storage, lipid nanoparticles generally show an increase in size and decrease in encapsulation (33,34). Nevertheless, the system remained well within the acceptable ranges of all parameters at 22°C, showing good stability upon storage at room temperature as well. However, because the storage stability

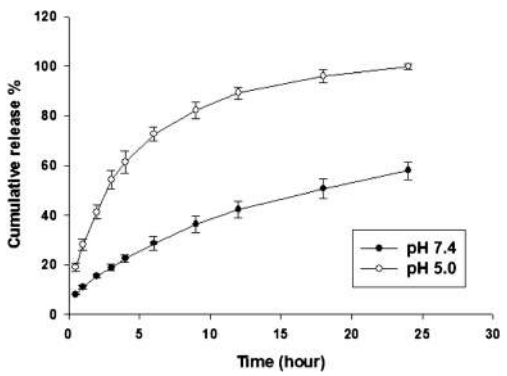

Fig. 6. *In vitro* drug release profile of the IMT-SLN system

Table IX. Correlation Coefficients and Rate Constants for Fitted *In Vitro* Release Models

Models	pH 7.4			pH 5.0		
	K	r^2	*n*	*K*	r^2	*n*
Zero order	2.1131	0.9508	–	4.2062	0.8199	–
First order	0.0746	0.7931	–	0.0770	0.6581	–
Higuchi	11.4985	0.9934	–	27.8201	0.8929	–
Korsmeyer-Peppas	11.0684	0.9979	0.5254	29.1222	0.9729	0.4652

K rate constant, r^2 correlation coefficient, *n* release exponent

was considerably better at 4°C, storage of IMT-SLN in a refrigerator at 4°C was recommended.

In Vitro Release Study

The *in vitro* release profiles of IMT from IMT-SLN at pH 7.4 and pH 5.0 are shown in Fig. 6. The cumulative drug release was expressed as percentage of total drug and demonstrated as a function of time. IMT-SLN showed a sustained drug release pattern at both pH 7.4 and pH 5.0. However, the rate of IMT release from IMT-SLN was markedly higher at pH 5.0, compared to pH 7.4. Tumor tissues have been reported to show pH levels in the acidic ranges, and the accelerated rate of drug release at lower pH indicates that IMT-SLN remains relatively stable in circulation while undergoing physicochemical changes inside tumor tissues to permit localized drug release inside the tumor environment (35,36).

The *in vitro* release data at pH 7.4 and pH 5.0 were fitted to four mathematical models: zero-order, first-order, Higuchi, and Korsmeyer-Peppas models using KinetDS 3.0 software. The respective rate constant (*K*) and correlation coefficient (r^2) values, along with the release exponent (*n*) values for the Korsmeyer-Peppas model, are shown in Table IX. Mathematical modeling of the *in vitro* release data demonstrated that IMT release from IMT-SLN followed the Korsmeyer-Peppas model, as indicated by the maximum corresponding r^2 values of 0.9979 and 0.9729 for release at pH 7.4 and pH 5.0, respectively. The release exponent (*n*) values of 0.5254 and 0.4652 (greater than 0.45) indicate that the drug release mechanism followed anomalous or non-Fickian diffusion, involving drug diffusion from the lipid core as well as erosion of the lipid core (37,38).

CONCLUSIONS

In the current study, a combination of two experimental design approaches was used for optimization and preparation of IMT-SLN: PBD for initial screening for identification of the most significant variables and BBD for optimization of the variables found to be significant by PBD. Use of the aforementioned experimental design approach enabled a clear understanding of the effects of various formulation variables on IMT-SLN characteristics and accurate prediction of the relationships between them and was thereby helpful in successfully optimizing the formulation variables for preparation of IMT-SLN showing excellent physicochemical and *in vitro* drug release characteristics.

ACKNOWLEDGMENTS

This research was supported by the National Research Foundation of Korea (NRF) grant funded by the Korea government (MSIP) (No. 2015R1A2A2A01004118, 2015R1A2A2A04004806). This work was also supported by the Medical Research Center Program (2015R1A5A2009124) through the NRF funded by MSIP.

REFERENCES

1. Deininger M, Buchdunger E, Druker BJ. The development of imatinib as a therapeutic agent for chronic myeloid leukemia. Blood. 2005;105:2640–53.
2. Al-Hadiya BMH, Bakheit AHH, Abd-Elgalil AA. Imatinib mesylate. In: Brittain HG, editor. Profiles of drug substances, excipients, and related methodology. San Diego: Elsevier Inc.; 2014. p. 265–97.
3. Harde H, Das M, Jain S. Solid lipid nanoparticles: an oral bioavailability enhancer vehicle. Expert Opin Drug Deliv. 2011;8:1407–24.
4. Gündüz H, Özlü Y, Yalçin S. Process for the preparation of imatinib base. US Patent No. US8252926 B2. 2012.
5. Müller RH, Mäder K, Gohla S. Solid lipid nanoparticles for controlled drug delivery—a review of the state of the art. Eur J Pharm Biopharm. 2000;50:161–77.
6. Mehnert W, Mäder K. Solid lipid nanoparticles: production, characterization and applications. Adv Drug Deliv Rev. 2001;47:165–96.
7. Wissing SA, Kayser O, Müller RH. Solid lipid nanoparticles for parenteral drug delivery. Adv Drug Deliv Rev. 2004;56:1257–72.
8. Üner M, Yener G. Importance of solid lipid nanoparticles (SLN) in various administration routes and future perspectives. Int J Nanomedicine. 2007;2:289–300.
9. Li H, Zhao X, Ma Y, Zhai G, Li L, Lou H. Enhancement of gastrointestinal absorption of quercetin by solid lipid nanoparticles. J Control Release. 2009;133:238–44.
10. Fonte P, Nogueira T, Gehm C, Ferreira D, Sarmento B. Chitosan-coated solid lipid nanoparticles enhance oral absorption of insulin. Drug Deliv Transl Res. 2011;1:299–308.
11. Lobovkina T, Jacobson GB, Gonzalez-Gonzalez E, Hickerson RP, Leake D, Kaspar RL, *et al*. In vivo sustained release of siRNA from solid lipid nanoparticles. ACS Nano. 2011;5:9977–83.
12. Montenegro L, Sinico C, Castangia I, Carbone C, Puglisi G. Idebenone-loaded solid lipid nanoparticles for drug delivery to the skin: in vitro evaluation. Int J Pharm. 2012;434:169–74.
13. Shi S, Han L, Deng L, Zhang Y, Shen H, Gong T, *et al*. Dual drug (microRNA-34a and paclitaxel)-loaded functional solid lipid nanoparticles for synergistic cancer cell suppression. J Control Release. 2014;194:228–37.
14. Pople PV, Singh KK. Development and evaluation of topical formulation containing solid lipid nanoparticles of vitamin A. AAPS PharmSciTech. 2006;7(4):E63–9.
15. Lionberger RA, Lee SL, Lee L, Raw A, Yu LX. Quality by design: concepts for ANDAs. AAPS J. 2008;10:268–76.

16. Poudel BK, Marasini N, Tran TH, Choi HG, Yong CS, Kim JO. Formulation, characterization and optimization of valsartan self-microemulsifying drug delivery system using statistical design of experiments. Chem Pharm Bull. 2012;60:1409–18.
17. Dejaegher B, Heyden YV. Experimental designs and their recent advances in set-up, data interpretation, and analytical applications. J Pharm Biomed Anal. 2011;56:141–58.
18. Gupta B, Poudel BK, Tran TH, Pradhan R, Cho HJ, Jeong JH, *et al*. Modulation of pharmacokinetic and cytotoxicity profile of imatinib base by employing optimized nanostructured lipid carriers. Pharm Res. 2015. doi:10.1007/s11095-015-1673-7.
19. Velpandian T, Mathur R, Agarwal NK, Arora B, Kumar L, Gupta SK. Development and validation of a simple liquid chromatographic method with ultraviolet detection for the determination of imatinib in biological samples. J Chromatogr B. 2004;804:431–4.
20. Ramasamy T, Khandasami US, Ruttala H, Shanmugam S. Development of solid lipid nanoparticles enriched hydrogels for topical delivery of anti-fungal agent. Macomol Res. 2012;20:682–92.
21. Wang S, Chen T, Chen R, Hu Y, Chen M, Wang Y. Emodin loaded solid lipid nanoparticles: preparation, characterization and antitumor activity studies. Int J Pharm. 2012;430:238–46.
22. Yuan Q, Han J, Cong W, Ge Y, Ma D, Dai Z, *et al*. Docetaxel-loaded solid lipid nanoparticles suppress breast cancer cells growth with reduced myelosuppression toxicity. Int J Nanomedicine. 2014;9:4829–46.
23. Das S, Chaudhury A. Recent advances in lipid nanoparticle formulations with solid matrix for oral drug delivery. AAPS PharmSciTech. 2011;12(1):62–76.
24. Derringer G, Suich R. Simultaneous optimization of several response variables. J Qual Technol. 1980;2:214–9.
25. Selvamuthukumar S, Velmurugan R. Nanostructured lipid carriers: a potential drug carrier for cancer chemotherapy. Lipids Health Dis. 2012;11:159–66.
26. Lainé AL, Gravier J, Henry M, Sancey L, Béjaud J, Pancani E, *et al*. Conventional versus stealth lipid nanoparticles: formulation and in vivo fate prediction through FRET monitoring. J Control Release. 2014;188:1–8.
27. Moghimi SM, Hunter AC, Murray JC. Long-circulating and target-specific nanoparticles: theory to practice. Pharmacol Rev. 2001;53:283–318.
28. Zhang C, Gu C, Peng F, Liu W, Wan J, Xu H, *et al*. Preparation and optimization of triptolide-loaded solid lipid nanoparticles for oral delivery with reduced gastric irritation. Molecules. 2013;18:13340–56.
29. Hao J, Fang X, Zhou Y, Wang J, Guo F, Li F, *et al*. Development and optimization of solid lipid nanoparticle formulation for ophthalmic delivery of chloramphenicol using a Box-Behnken design. Int J Nanomedicine. 2011;6:683–92.
30. Shah MK, Madan P, Lin S. Preparation, in vitro evaluation and statistical optimization of carvedilol-loaded solid lipid nanoparticles for lymphatic absorption via oral administration. Pharm Dev Technol. 2014;19:475–85.
31. Zhang X, Liu J, Qiao H, Liu H, Ni J, Zhang W, *et al*. Formulation optimization of dihydroartemisinin nanostructured lipid carrier using response surface methodology. Powder Technol. 2010;197:120–8.
32. Sofou S. Radionuclide carriers for targeting of cancer. Int J Nanomedicine. 2008;3:181–99.
33. Tran TH, Ramasamy T, Truong DH, Shin BS, Choi HG, Yong CS, *et al*. Development of vorinostat-loaded solid lipid nanoparticles to enhance pharmacokinetics and efficacy against multidrug-resistant cancer cells. Pharm Res. 2014;31:1978–88.
34. Zhang XY, Qiao H, Ni JM, Shi YB, Qiang Y. Preparation of isoliquiritigenin-loaded nanostructured lipid carrier and the in vivo evaluation in tumor-bearing mice. Eur J Pharm Sci. 2013;49:411–22.
35. Shen Y, Tang H, Radosz M, Van Kirk E, Murdoch WJ. pH-responsive nanoparticles for cancer drug delivery. In: Jain KK, editor. Drug delivery systems (methods in molecular biology). New Jersey: Humana Press; 2008. p. 183–216.
36. Gao W, Chan J, Farokhzad OC. pH-responsive nanoparticles for drug delivery. Mol Pharm. 2010;7:1913–20.
37. Pradhan R, Kim Y, Chang SW, Kim JO. Preparation and evaluation of once-daily sustained-release coated tablets of tolterodine-L-tartrate. Int J Pharm. 2014;460:205–11.
38. Arora G, Malik K, Singh I, Arora S, Rana V. Formulation and evaluation of controlled release matrix mucoadhesive tablets of domperidone using *Salvia plebeian* gum. J Adv Pharm Technol Res. 2011;2:163–9.